Proceedings of Global Power and Propulsion Society
ISSN-Nr: 2504-4400
GPPS Xi'an21
18th – 20th October, 2021
www.gpps.global

GPPS-TC-2021-0012

EFFECT OF CIRCUMFERENTIAL SINGLE CASING GROOVE LOCATION ON THE FLOW STABILITY UNDER TIP CLEARANCE EFFECT IN A TRANSONIC AXIAL FLOW COMPRESSOR ROTOR

Zonghao Yang
School of Power and Energy, Northwestern Polytechnical University
yangzonghao@mail.nwpu.edu.cn
Xi'an, Shaanxi, China

Xiaoxiong Wu
School of Power and Energy, Northwestern Polytechnical University
wxx1990@mail.nwpu.edu.cn
Xi'an, Shaanxi, China

Xiaochen Mao*
School of Power and Energy, Northwestern Polytechnical University
maoxiao_chen@nwpu.edu.cn
Xi'an, Shaanxi, China
*Corresponding author

Bo Liu
School of Power and Energy, Northwestern Polytechnical University
liubo704@nwpu.edu.cn
Xi'an, Shaanxi, China

ABSTRACT

The effects of different axial locations of circumferential single groove casing treatment (CT) schemes on the flow field stability of the transonic compressor rotors with three tip clearance sizes (TCS) are studied numerically, and the corresponding control mechanisms are performed. From the results, it can be seen that placing grooves at 10% to 40% of the axial chord length of the blade tip will make CT more efficient, and among the three TCS schemes, the G2 scheme located at near 20% of the blade tip axial chord length is the best CT scheme to improve the stall margin.For the effective CTs, the tip leakage flow (TLF) intensity, entropy generation and tip flow blockage are all reduced, so the area between the mainstream of the incoming stream and TLF moves downward. Quantitative analysis of relative inlet flow angle indicates that for this transonic rotor, reducing the flow incidence angle does not necessarily improve the flow stability. Control mechanism may be different for different TCS schemes due to the distinction of stall inception process. For a better application of CT, the blade tip profile should be further modified by using optimization method to adjust the shock position and strength during the design of a more efficient CT.

1.INTRODUCTION

As we all know, the rotor tip leakage flow (TLF) has a significant impact on the efficiency, pressure rise capacity and safe operation of the compressor (Koch and Smith, 1976). Generally, TLF often exists in the tip region in a form of tip leakage vortex (TLV). In transonic compressors, the interaction between the passage shock wave, secondary flow and TLF/TLV can make the tip flow more complicated. In the past few decades, a lot of research has been done on the TLF flow mechanisms and the tip clearance effect. (Khalid et al., 1999).

As an effective approach to reduce the detrimental effect of aerodynamic instabilities, the casing treatment is very effective in increasing the working stability of the aero-engine compression system. The development of a range of different CTs in compressors was best depicted by Hathaway (2007). Additionally, compared with slot-based CT, a grooved CT can offer better mechanical integrity with less impact on the compressor efficiency. In order to make the groove design more perfect, researchers have conducted a lot of investigations on the corresponding mechanism of groove CT to enhance flow stability (Shabbir et al., 2005). The results show that the compressor is greatly affected by the rotor TLF during the initiation of the stall, and the compressor stall margin improvement (SMI) strongly correlates with the mutual influence of casing groove and rotor tip flow.

The investigation on CT effect and its corresponding contribution to the SMI with single groove is an effective way to reveal the flow control mechanism of grooved CT. Some researchers made a single groove at different positions of the subsonic compressor to explore the relevant mechanism of the position of a single groove CT

to improve the flow stability of the compressor (Liu et al., 2016; Mao et al., 2018). For transonic compressors, Sakuma et al. (2014) and Mirzabozorg et al. (2017) have numerically studied how circumferential single-slot CTs can improve compressor stability. However, Researchers are divided on how to set the groove to the best position to make it effectively improve the compressor performance, because the stall inception process and the groove working principles are not fully understood. Therefore, more research efforts should be spent to study the effect of the axial position of single groove CT on the SMI and the corresponding mechanism.

With the design of modern axial compressors trending toward higher pressure ratio, the rotor relative tip clearance becomes larger due to the lower annulus height and smaller blades in the compressor later stages. Additionally, transient operations and thermal expansion can also lead to a change of rotor tip clearance. At present, the treatment of the casing of the circumferential groove is also under study to eliminate or relieve the negative effect associated with an increase of rotor tip clearance. Tsukuda (1977) studied the effect of circumferential groove CT under different tip clearances on the performance of low-speed compressors. The results indicated that the effect of the groove is the most obvious at the small tip clearance. Rolfes et al. (2017) experimentally found that in a low-speed axial compressor, the advantage of the circumferential groove CT to expand the working range of the compressor at the small blade tip gap is very small, however, when there is a large tip clearance, the compressor stall margin and efficiency are improved. With the help of simulations, Hamzezade et al. (2019) also found that a circumferential groove CT placed near the trailing edge of the first-stage rotor will have a better effect with a larger blade tip clearance size in a multistage axial compressor. The numerical parameters of the coupling between the tip clearance and the circumferential groove are studied in a transonic axial flow compressor by Beheshti et al. (2004). They also found that the circumferential groove CTs have a better effect when the tip gap is large. Cevik et al. (2016) numerically found that a proper designed circumferential groove CT can reduce the sensitivity of performance and stall margin to tip clearance in a high-speed subsonic axial flow compressor. A similar conclusion was also observed by Fujita and Takata (1984) in a low speed compressor. However, in the rotor of a transonic compressor that considers the tip clearance effect, there are few related studies on the influence of the position of a single groove CT on the tip flow stability.

Therefore, under the influence of the tip clearance of the rotor of a transonic compressor, the present work will study the influence of setting a single groove CT at different positions on the flow stability of the tip. The current paper will conduct research from the following two aspects. First, based on the SMI under three different blade tip clearances, the axial position of a single casing groove was studied parametrically. Second, Analyze the results of the parameter study, mainly including the variation of the tip flow characteristics and the corresponding control mechanism. The organization of this paper is as follows. Firstly, the compressor rotor, the numerical method and the numerical verification are explained in the second and third sections respectively. Then the numerical results are analyzed in detail in the fourth section. Finally, the conclusion of the analysis is summarized in fifth section.

2.1 Transonic compressor rotor

The test case studied in this paper is a high-speed axial compressor rotor of the NASA Stage35 (Reid et al., 1978). Figure 1 shows the cross-sectional diagram of the transonic compressor stage. The detailed aerodynamic design parameters of the rotor are listed in Table 1.

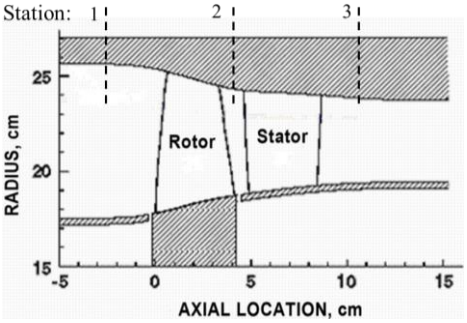

Figure 1 Schematic diagram of the transonic compressor stage

Table 1 Main design parameters of the transonic rotor

Design parameter	Value	Unit
Mass flow rate	20.2	kg/s
Pressure ratio	1.8	[-]
Number of blades	36	[-]
Rotational speed/rpm	17188.7	rpm
Relative tip speed	454.5	m/s
Tip clearance	0.408	mm
Aspect ratio	1.19	[-]

2.2 Design of circumferential grooved CTs

For each of the three different tip clearance size (TCS) schemes, this paper studies eleven circumferential single grooves which over the blade tip. The three different TCS schemes are τ, 1.5τ and 2τ (τ corresponds to the design TCS). Therefore, a total of thirty-three casing groove schemes were investigated in this work. From Fig. 2 we can see the circumferential groove CT located on the upper end wall, and the grid near the groove can also be seen in the lower right of Fig. 2. At the same time, the position of a single groove is defined in the upper right of Figure 2, that is, the axial distance from the leading edge (LE) of the blade to the leading edge of the

groove, and this distance is normalized by the axial chord length at the tip of the blade. The height (d) and width (w) of the groove designed in this paper are 4mm and 2mm respectively, so the aspect ratio (AR) is 2 which is the same as that in Houghton et al. (2011). Using the software of IGG (NUMECA International, 2009) to generate a single groove mesh in H topology, it has a total of 0.65×10^5 nodes, and the number of nodes in the axial, radial and tangential directions are 21, 45, and 69, respectively. The full non-matching connecting technology was used to connect the mesh of a casing groove and the main blade passage.

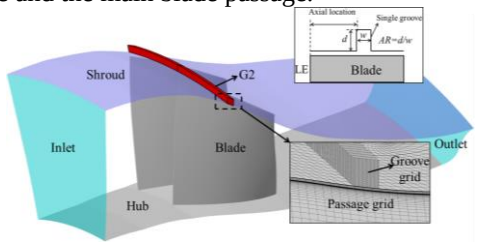

Figure 2 Schematic of a circumferential grooved CT and the zoomed view of the grid near the groove

3. NUMERICAL APPROACH AND VALIDATION

The commercial RANS solver FINE/TURBO was used for the numerical simulations in this paper. Single passage steady simulations were performed by using the periodical boundary conditions. An explicit four-order Runge-Kutta scheme was employed for the temporal discretization and used a cell-centered finite volume scheme for the spatial discretization. Taking into account the internal turbulent flow, the Spallart–Almaras turbulence model was used.

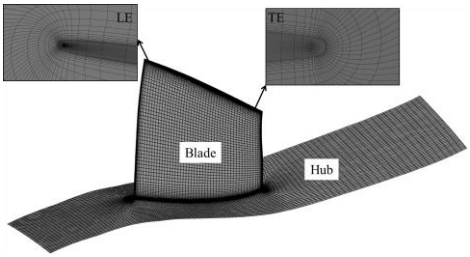

Figure 3 The computational mesh of the compressor rotor

The Autogrid5 module divided the main passage of the blade into the O4H topological structure, and used butterfly grid technology at the blade tip gap to improve the quality of grid generation. Figure 3 shows the lower end wall (Hub) of the cascade and the mesh of the blade, and shows an enlarged view of the partial mesh of the leading edge (LE) and trailing edge (TE) of the blade tip.To ensure the accuracy of numerical predictions, the grid setup for the blade passage is similar with that in Ref. in spanwise, streamwise and tangential directions. There are 17 nodes for the design rotor tip gap and the number of grid node was increased for the larger tip clearances. The total number of grids of the blade passage is set to 1.03×10^6. The mesh size of the first layer of the near-solid wall is set to 5×10^{-6} m, so that the dimensionless parameter $y+\leq3$, so as to meet the numerical calculation requirements of the turbulence model selected in this paper.

In the computations, the inlet boundary conditions were given as total pressure, total temperature and inlet airflow angle. The static pressure near mid-span was specified by a simple radial equilibrium law at the outlet plane. The boundary condition of the solid wall was no slip and adiabatic.

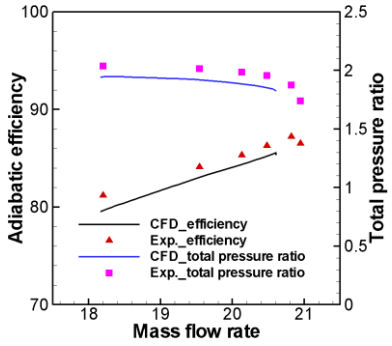

Figure 4 Comparison of the calculated and experimental overall performance

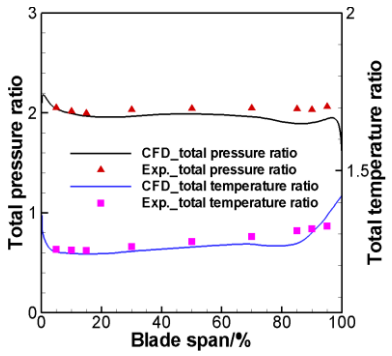

Figure 5 Comparison of pitch-averaged total pressure ratio and total temperature ratio

In order to verify the reliability of the numerical calculation method used in this research, Figure 4 shows the comparison between the overall performance of the numerical calculation and the experiment at the design speed condition. As the mass flow rate decreased, the last convergence point in the calculation determined the limit of numerical stability. In order to predict the stall margin accurately, back pressure dichotomy method was used in the computations (Gao et al., 2012). From Figure 4, although there is discrepancy for the mass flow rate at the choke condition between the numerical and experimental results, within the maximum working range, the numerical results have the same trend as the experimental results, and the stall point predicted by the numerical calculation is very close to the experimental results. As shown in Figure 5, at the near-stall condition of 18.21 kg/s, the total pressure ratio and total temperature ratio of the numerical results were pitch-averaged and compared with the experimental results. Both the pitch-averaged total pressure ratio and total temperature ratio are obtained at the Station 2 shown in Figure 1. It can be seen that the

predicted value and the experimental result are close to each other. Therefore, the numerical method can make a good prediction of the overall performance and flow details with a sufficient reliability on the whole, which makes us confident to use this calculation method to draw conclusions about the CT effect.

4. RESULTS AND DISCUSSION

4.1 Effect of CTs on the stall margin improvement

The parameter study of the axial position of a single casing groove was carried out, and eleven circumferential single grooves were investigatived for each of the three different TCS schemes (τ, 1.5τ and 2τ). In this work, the axial position of the groove determines the naming of each CT configuration. For example, G2 means that the distance between the leading edge of the groove and the leading edge of the blade is 20% of the axial chord length of the blade tip.

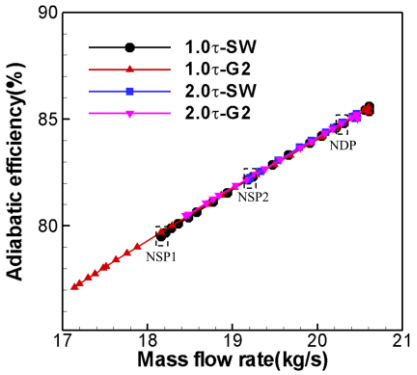

(a) Adiabatic efficiency performance curve

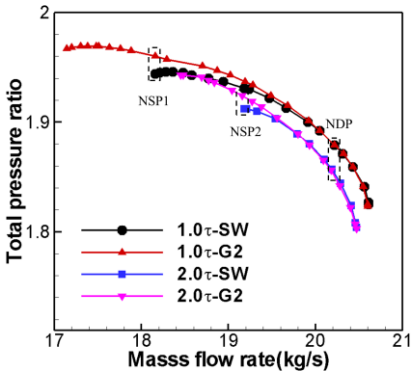

(b) Total pressure ratio performance curve

Figure 6 Overall characteristics plots for the CT scheme of G2 at two different TCS schemes

For conciseness, only the overall performance of the best CT schemes at two different TCS scheme are presented here. At the tip gaps between τ and 2τ, the efficiency and total pressure characteristics of the CT scheme of G2 are calculated, as shown in Figure 6. In both the TCS schemes, the mass flow rate at the stall point of G2 is significantly lower than that of the smooth wall (SW) case. It should be mentioned that the efficiency of the CT schemes are increased for the two TCS schemes due to the improvement of tip flow field at the near stall point of the SW case (NSP1 and NSP2 correspond to the near stall condition of the SW case at the TCS of τ and 2τ respectively), especially for the TCS of τ. However, there is almost no efficiency change for the CT schemes at the near design point (NDP). Additionally, the change of the adiabatic efficiency curve in the whole flow range is similar to the change of the total pressure ratio curve.

In the current work, the effect of the CT scheme is evaluated by the improvement of stall margin (SMI), which is defined as the following equation:

$$SMI = [\frac{\pi_{stall} m_{design}}{\pi_{design} m_{stall}} - 1]_{CT} - [\frac{\pi_{stall} m_{design}}{\pi_{design} m_{stall}} - 1]_{SW} \quad (1)$$

Figure 7 presents the calculated SMI for each groove configuration at three different TCS schemes. One can see that the CT is better to increase the flow stability that the grooves are located from 10% to 40% tip axial chord, and G2 is the best CT scheme for all the three TCS schemes. The SMI decreases as the groove location is shifted downstream from the position of 20% tip axial chord. The best scheme of G2 increases the stall margin by about 8.3%, 8.2% and 6.2% at the TCS of τ, 1.5τ and 2τ respectively. Due to the error of the stall point in the stable single-channel calculation, the change of the CTs after 50% tip axial chord and near the leading edge on the SMI seems insignificant. Compared with the TCS of τ, the SMI keeps almost unchanged when the casing grooves are located at the position of 10% and 20% tip axial chord at the TCS of 1.5τ, while the SMI is slightly higher for other CT schemes. As the TCS is increased to 2τ, the SMI is reduced obviously before the position of 30% tip axial chord. However, there is no remarkable change of SMI at the position of 30% and 40% tip axial chord. Overall, the CT schemes are most effective at the TCS of 1.5τ.

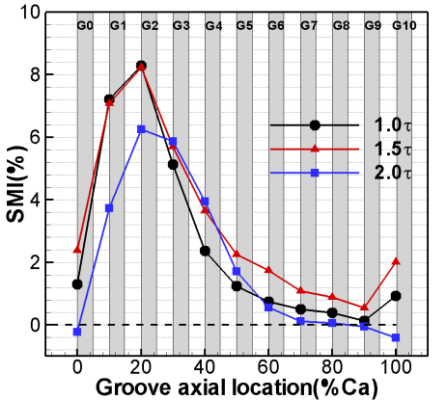

Figure 7 SMI trends as a function of groove location at three different TCS schemes

The sensitivity results of SMI to tip clearance for the four more efficient CT schemes (G2, G3, G4 and G5) are shown in Figure 8. It can be seen the sensitivity of SMI is lowest for G3 compared with other CT schemes and G4 is another better option. At the TCS of 2τ, the SMI of G3

(5.9%) is only slightly lower than the best CT scheme of G2 (6.2%). Therefore, the CT scheme of G2 is the best choice to ameliorate the flow stability without considering the sensitivity of SMI within a certain range of TCS variation. However, the CT schemes of G3 and G4 may be two better options to reduce the effect of the sensitivity of SMI during the design of CT scheme with multi-grooves based on the CT of G2.

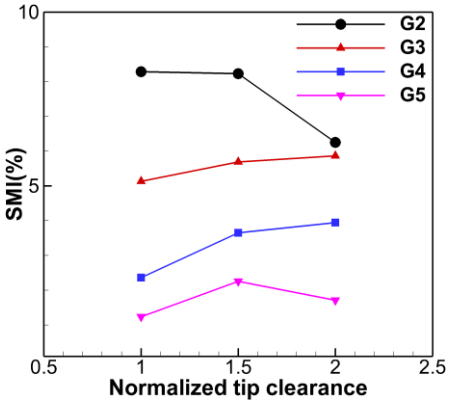

Figure 8 Sensitivity results of SMI for four different CT schemes

4.2 Effect of CTs on the tip flow behaviors

As we all know, TLF is very important in the initiation of the stall near the tip of the blade. Therefore, the effect of CT on the tip flow field and the corresponding mechanism will be analyzed at two TCS schemes in this section. The best CT scheme of G2 and the SW case will be selected to explore the impact of CT at the TCS schemes of τ and 2τ in detail. Perform detailed analysis under near stall conditions (NSP1 for TCS of τ, and NSP2 for TCS of 2τ) which has been marked in Figure 6.

The entropy contours on the plane of blade tip at the near stall condition are compared in Figure 9. It has been shown that the downward movement of the interface which between the TLF and incoming main airflow can be used to check the enhancement of flow stability (Vo et al., 2008; Cameron et al., 2013). Generally, The entropy contour can be used to depict the interface as a high gradient area, and it is drawn with a black dashed line in Figure 9. Souleimani et al. (2018) also stated that spike stall inception occurs when the interface appears on the plane of the leading edge of the blade tip. If not (i.e. the interface position is yet in the blade channel), modal stall inception can be inferred. Therefore, these two criteria will be used in the following analysis as well.

For the TCS of τ, the interface of the SW case is only located at the leading edge of blade that indicates that spike stall inception may occur with further mass flow rate reduced. In the CT scheme, it can be seen that the interface obviously moves downstream of the flow passage, which means that the safe operating range is improved. From the change of entropy contour in G2, the loss generation close to blade leading edge is decreased obviously due to the improvement of TLF with the help of casing groove. However, the loss generation is increased on the blade suction surface which close to the trailing edge indicated by black oval, and it means that airflow of the tip structure may be changed after the use of CT at the TCS of τ.

As the TCS is increased to 2τ, it can be seen that the interface position of the SW case hardly changes, so we can infer that the modal stall inception may happen at a lower mass flow rate. The interface is also shifted further downstream for the CT, which indicates that the flow stability is also enhanced with the help of casing groove. The slight reduction of entropy shows that the impact of TLF is decreased and the flow filed is improved to some extent. The reduction of loss closs to the blade tip after the use of CT at both TCS schemes is consistent with the result that compressor performance becomes better at close to stall condition for the CTs shown in Figure 6.

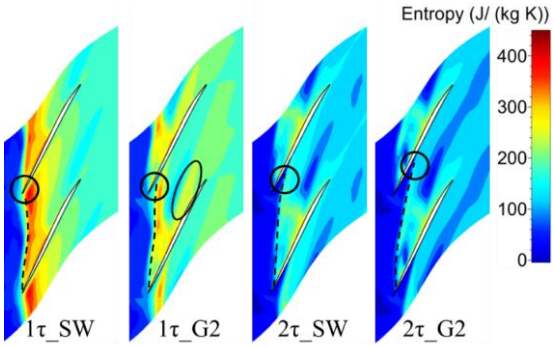

Figure 9 Entropy contours on the blade tip plane

As shown in Figure 10, the shock wave position is also marked with black line in the figure. For the SW case at the TCS of τ, one can observe that there exists a low energy fluid area at the pressure side which close to the blade leading edge caused by the interaction between the TLF and shock wave. After the CT, the low energy fluid area is reduced obviously, and it associates with the reduction of loss generation near the blade leading edge shown in Figure 9. For this reason, the tip airflow blockage is reduced, which is beneficial to the SMI. In addition, the shock wave is shifted downstream obviously and its intensity becomes stronger which can be seen from the higher Mach number before the sonic line near the blade suction side. The boundary layer on the blade suction surface is separated due to the stronger interaction between the shock wave and low energy boundary layer, which is consistent with the increase of loss generation. Although the tip flow blockage is increased due to the boundary layer separation, the flow capacity is improved indeed obviously because of the disappearance of the low energy fluid region at the pressure side. However, Figure

10 shows that there is hardly change of tip airflow structure after the CT at the TCS of 2τ.

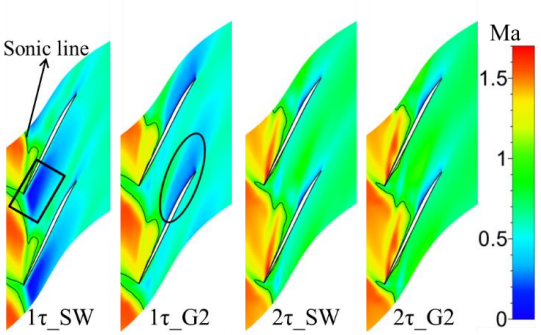

Figure 10 Relative Mach number contours on the blade tip plane

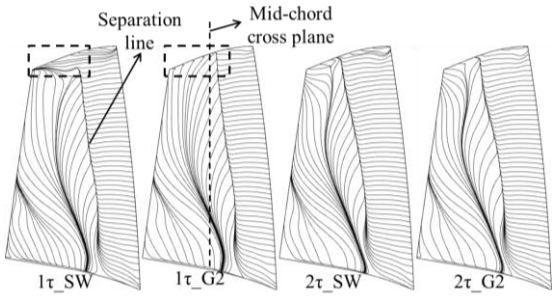

Figure 11 Limiting streamlines on the blade suction surface

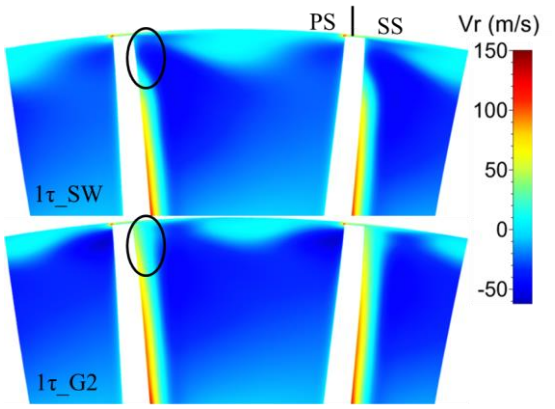

Figure 12 Radial velocity contours on the mid-chord cross plane at the TCS of τ

It can be observed from Figure 11 that the CT has remarkable influence on the tip flow structure at the TCS of τ, while there has no obvious change of tip airflow structure at the TCS of 2τ after CT. For the TCS of τ, there is no separation line near the blade tip caused by the interaction between the wave shock and boundary layer in the SW case. However, after CT, the separated boundary layer induced by the stronger shock wave tends to migrate toward the blade tip under the centrifugal force. Figure 12 shows the radial velocity contours on the mid-chord cross plane (indicated as Figure 11) at the TCS of τ. The radial velocity close to blade tip which marked by black oval increases remarkably after the CT. For this reason, additional mixing loss may occur caused by the TLF and the climbing boundary layer separation. Therefore, for a better application of CT, the blade tip profile should be modified by using optimization method to adjust the shock position and strength during the design of CT.

Rabe and Hah (2002) indicated that the casing groove increases the stall margin by decreasing the angle of incidence of the airflow in a transonic compressor. It is also widely accepted that the flow incidence angle becomes larger and larger in pace with the mass flow rate is reduced gradually. Therefore, the reduction of incoming flow incidence angle may be beneficial to gas flowing. The spanwise distribution of pitch-averaged relative flow angle at the rotor inlet plane is plotted in Figure 13. It should be mentioned that the variation trend of the flow incidence angle is the same as the change of the relative inlet flow angle considering the unchanged blade stagger angle. For the TCS of τ, the incidence angle which close to the blade tip is decreased slightly (about 1 degree) after CT, which relates to the increase of tip airflow capacity due to the decrease of airflow blockage. However, there is almost no change of incidence angle after CT at the TCS of 2τ. Therefore, it seems that the decrease of flow incidence angle is not necessary to improve flow stability for transonic rotor in this paper.

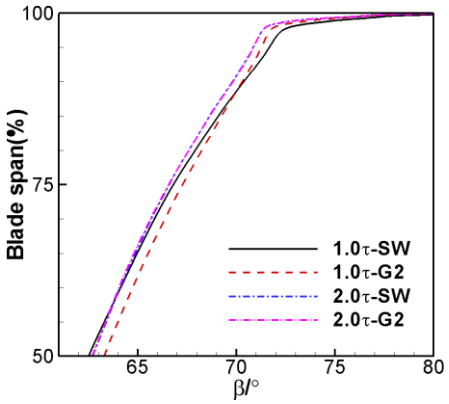

Figure 13 Spanwise distribution of pitch-averaged relative flow angle at the rotor inlet plane

Studies have shown that there is an angle between the TLF at the tip clearance exit and the mainstream, and the strength of the local TLF can be measured by this angle. Generally, the larger the angle, the more likely a double leakage flow phenomenon will occur (Beheshti et al., 2004). Khalid et al. also showed that double leakage flow can affect flow blockage and loss generation (Khalid et al., 1999). Thus, the tip leakage flow angle (TLA) which between axial direction and TLF exit direction is utilized to investigate the strength change of the TLF and double leakage flow here.

It can be seen from Figure 14 that compared with the SW program, tip leakage flow angle in both TCS schemes decreases apparently in almost the whole blade after CT, in particular within the front part of blade except for the

location close to blade leading edge. Actually, the decrease of tip leakage angle is more obvious under groove position and within a certain blade chord range just behind the groove, especially for the TCS of τ. Therefore, local TLF intensity decrease after CT for both TCS schemes and the risk to cause the double leakage flow also decrease, and it is good to the enhancement of flow stability and compressor performance at the near stall point. Additionally, unlike the TCS of τ, there is no change of tip leakage angle near the blade leading edge at the TCS of 2τ after the CT of G2, and it is the same as the unchanged incoming airflow incidence angle shown in Figure 13.

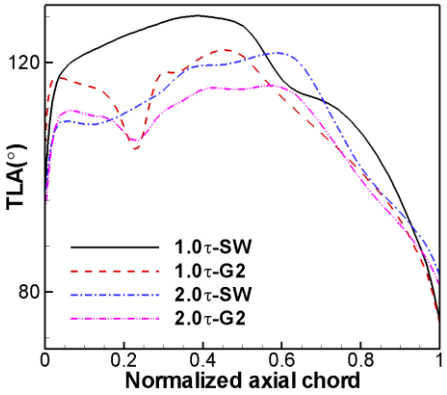

Figure 14 Distributions of tip leakage flow angle at mid-gap

In general, the value of absolute vorticity is used for evaluating the strength of TLF. The normalized absolute vorticity is defined as the equation below:

$$\xi_n = \frac{|\xi|}{2\omega} \tag{2}$$

$|\xi|$ represents the magnitude of the absolute vorticity vector in the formula and ω represents angular velocity of the rotor. The pitch-averaged normalized absolute vorticity contours on the meridional plane together with streamline distribution is shown in Figure 15, in which the vertical red dashed lines represent the axial location of the vortex core in the SW case at the two TCS schemes.

For the TCS of τ, compared with the SW case, the maximum value and the high vorticity area are decreased obviously after the CT, which means that the intensity of TLF is reduced and the tip flow area get better with the help of groove. In addition, the original vortex is separated into two parts and the vortex core of the new larger vortex is shifted downstream obviously, which indicates that the tip airflow structure is changed after CT. For the TCS of 2τ, both the peak value and the high vorticity area are also decreased after CT. Therefore, tip flow area at the TCS of 2τ is also ameliorated by the CT. However, there is no obvious variation of tip flow structure and only the vortex core is shifted downstream slightly. Overall, these results are consistent with the analysis above.

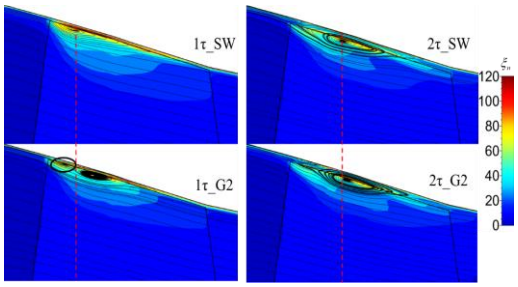

Figure 15 Pitch-averaged normalized absolute vorticity contours on the meridional plane

Figure 16 compares entropy contours on the mid-chord cross plane. At the TCS of τ, due to the upward migration of boundary layer separation by the shock wave interaction, the loss generation marked by black oval is increased obviously after CT compared with the SW. However, both the peak value and high entropy area caused by the TLV are decreased remarkably, and it relates to the improvement of tip flow filed after CT. For the TCS of 2τ, compared with the SW, the high entropy region and the peak value due to the impact of TLV are also decreased after CT, which relates to the decrease of TLF intensity.

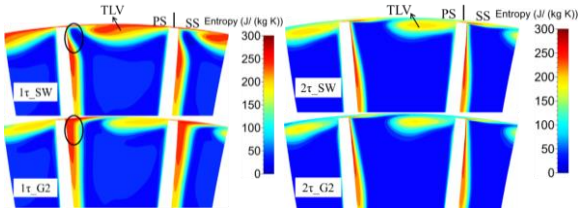

Figure 16 Entropy contours on the mid-chord cross plane

From Du et al. (2013), it indicated that the TLF of the transonic rotor can be divided into different parts along the chordwise, which plays a different role in the stall inception process. To gain a better insight into the impact of CT on the clearance flow behaviors in this transonic rotor, the three-dimensional flow streamlines over two important blade chord range are used to analyze the CT effect according to the flow features, i.e., LE-20% tip axial chord (denoted as the front part), 20%–70% tip axial chord (denoted as the middle part). The front part mainly determines the initial interface position near the blade suction surface, while the middle part pushes the interface upstream after intersecting with the incoming flow near the pressure side of the adjacent blade.

Figure 17 shows the flow streamlines colored with relative Mach number, which released from the blade LE to 20% tip axial chord at the TCS of τ. In the SW case, a breakdown of TLV occurs due to the TLV/shock wave interaction. As a result, a large low-speed flow region happens and a severe flow blockage occurs near the adjacent blade pressure side, which leads to a remarkable local loss generation. Then, a portion of the front part TLF

reaches to the adjacent blade tip and double leakage happens. The other portion flows directly out of the passage. After the CT, the TLV breakdown disappears and the tip flow field is modified significantly because the blockage is reduced. In addition, the phenomenon of double leakage is also alleviated slightly.

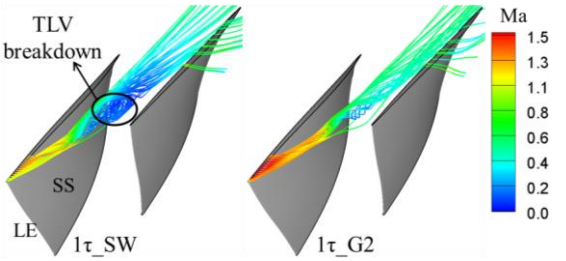

Figure 17 Three-dimensional flow streamlines released from the blade LE-20% tip axial chord at the TCS of τ

The three-dimensional flow streamlines in Figure 17 are re-colored with normalized helicity, as shown in Figure 18. The normalized helicity has been used to study the TLV breakdown phenomenon by Furukawa et al. (1999), which could identify the vortex core and show the swirl direction, and it can be defined as the equation below:

$$H_n = \frac{\xi \cdot w}{|\xi||w|} \tag{3}$$

where ξ and w are the vectors of the absolute vorticity and relative velocity respectively.

It can be observed that the normalized helicity marked by the black oval after the TLV/shock wave interaction changes drastically. The normalized helicity changes rapidly from +1 to -1, which means the occurrence of the TLV breakdown. The normalized helicity becomes positive again downstream of the TLV breakdown area. After the CT, there is no drastic change of the sign of the normalized helicity after the interaction of shock wave. Thus, the tip flow filed is improved due to the disappearance of the TLV breakdown. It has been found that the flow blockage due to the TLV breakdown has a important impact on the compressor stall inception (Furukawa et al., 1999; Schlechtriem et al., 1997). The disappearance of the vortex breakdown was also observed by Sakuma et al. (2014) after the application of circumferential grooved CT. Therefore, at the TCS of τ, the compressor flow stability can be enhanced by the suppression of the TLV breakdown caused by the shock wave/TLF interaction. In this way, the tip flow blockage is reduced and the likelihood of occurrence of interface spillage is decreased, which is beneficial to the SMI.

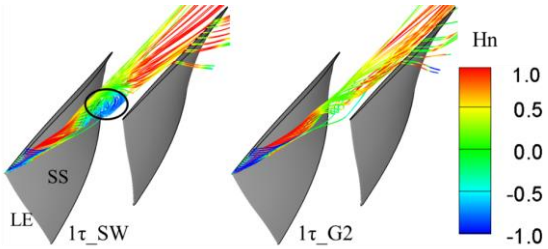

Figure 18 Three-dimensional flow streamlines released from the blade LE-20% tip axial chord colored with normalized helicity at the TCS of τ

Figure 19 shows the three-dimensional flow streamlines at the TCS of τ, which released from the 20% to 70% tip axial chord. For the SW case, a large portion of the middle part TLF impactsthe pressure side within the front part chord range of the adjacent blade and the double leakage phenomenon happens. The interface is almost parallel to the leading plane near the pressure side of the adjacent blade and the interface spillage will occur for a slightly lower mass flow rate. After CT, the double leakage phenomenon is almost removed from the blade leading edge, and the risk of interface spillage is reduced obviously which corresponds to the downward movement of the interface.

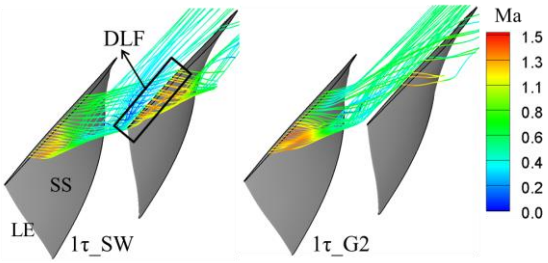

Figure 19 Three-dimensional flow streamlines released from the 20%-70% tip axial chord at the TCS of τ

The three-dimensional flow streamlines through the blade LE-70% tip axial chord at the TCS of 2τ are shown in Figure 20. Compared with the TCS of τ, one can observe that the TLV breakdown does not occur after the interaction between the front part TLF and shock wave in the SW case. Additionally, there are also no phenomenon of double leakage flow, and the interface is still located behind the blade leading edge. After CT, the TLF is further away from the pressure side of the adjacent blade near the leading edge, which means that the interface position is shifted more downstream due to the groove effect. In addition, the phenomenon of double leakage is relieved to some extent within the rear half blade chord range. The TLF intensity is also decreased thereby, which is beneficial to the SMI.

From the analysis above, the tip flow structure is changed after the CT of G2 at the TCS of τ. The effects of casing groove on TLF are different for the leakage flow released from different chord range. For the front part TLF, the TLV breakdown phenomenon disappears and the flow blockage near the blade tip is decreased

obviously, which reduces the risk of interface spillage at the blade leading edge. However, the double leakage phenomenon is almost removed near the blade leading edge due to the groove effect on the middle part TLF. The improvement of both the two different parts TLF contributes to the reduction of TLF intensity after the use of CT, which resulting in the flow stability enhancement. At the TCS of 2τ, no obvious change of flow structure after CT of G2 has been done, only the interface position is shifted more downstream with the help of the groove. Figure 9 shows that there are different stall inception process for the TCS schemes of τ and 2τ. Therefore, according to the change of tip flow structure, it can be concluded that the control mechanisms of CT may be different for various TCS schemes due to the distinction of stall inception process, which will be researched by performing corresponding high-fidelity multi-passage unsteady simulations.

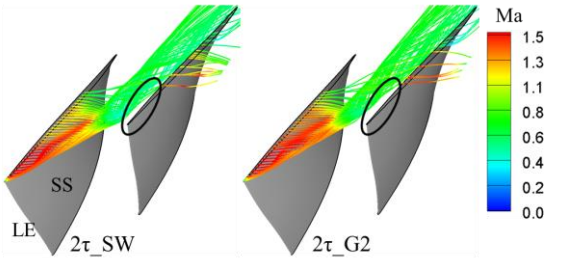

Figure 20 Three-dimensional flow streamlines released from the blade LE-70% tip axial chord at the TCS of 2τ

5. CONCLUSIONS

In this paper, numerical computations performed to study the effect of circumferential single grooved CT on the tip flow stability and corresponding control mechanism under tip clearance effect in a transonic axial flow compressor rotor. The conclusions are summarized as follows:

(1) Parametric study indicates that the CT schemes are most effective at the TCS of 1.5τ. It is more efficient to improve the flow stability when the grooves are located from 10% to 40% tip axial chord and G2 is the best CT scheme for all the three TCS schemes in terms of the SMI.

(2) The interface location is shifted downwards after the effective CTs. The TLF intensity, the entropy generation and tip flow blockage are all decreased to a different extent, which are beneficial to the SMI. The quantitative analysis of the relative inlet flow angle shows that the reduction of flow incidence angle is not necessary to improve the flow stability for the transonic rotor in this paper.

(3) The control mechanisms of CT may be different for different TCS schemes due to the distinction of the stall inception process. For a better application of CT, the blade tip profile should be modified by using optimization method to adjust the shock position and strength during the design of more efficient CT. In this way, the impact of new negative tip flow phenomenon (e.g., boundary layer separation induced by the stronger shock wave) can be relieved after the application of casing groove.

NOMENCLATURE

Symbols

β	Relative flow angle
m	Mass flow rate
w	Relative flow velocity
π	Total pressure ratio
τ	Design tip clearance
ξ	Absolute vorticity vector
ξ_n	Normalized absolute vorticity
H_n	Normalized helicity

Abbreviations

AR	Aspect ratio
CT	Casing treatment
LE	Leading edge
NDP	Near design point
NSP	Near stall point
PS	Pressure surface
SMI	Stall margin improvement
SS	Suction surface
SW	Smooth wall
TCS	Tip clearance size
TE	Trailing edge
TLA	Tip leakage flow angle
TLF	Tip leakage flow
TLV	Tip leakage vortex

ACKNOWLEDGMENTS

Thanks to the National Science and Technology Major Project (2017-II-0001-0013) and the National Natural Science Foundation of China (51790512) for funding this work.

REFERENCES

Koch C C, Smith L H. Loss sources and magnitudes in axial-flow compressors[J]. Journal of Engineering for Power, 1976, 98(3): 411-424.

Khalid S A, Khalsa A S, Waitz I A, et al. Endwall blockage in axial compressors[J]. Journal of Turbomachinery, 1999, 121(3): 499-509.

Hathaway M D. Passive endwall treatments for enhancing stability[R]. NASA Technical Paper, No. TM-214409, 2007.

Fujita H, Takata H. A study on configurations of casing treatment for axial flow compressors[J]. Bulletin of JSME, 1984, 27(230): 1675-1681.

Shabbir A, Adamczyk J J. Flow mechanism for stall margin improvement due to circumferential casing grooves on axial compressors[J]. Journal of turbomachinery, 2005, 127(4): 708-717.

Houghton T, Day I. Enhancing the stability of subsonic compressors using casing grooves[J]. Journal of Turbomachinery, 2011, 133(2): 021007.

Liu L, Li J, Nan X, et al. The stall inceptions in an axial compressor with single circumferential groove casing treatment at different axial locations[J]. Aerospace Science and Technology, 2016, 59: 145-154.

Mao X, Liu B, Tang T, et al. The impact of casing groove location on the flow instability in a counter-rotating axial flow compressor[J]. Aerospace Science and Technology, 2018, 76: 250-259.

Sakuma Y, Watanabe T, Himeno T, et al. Numerical analysis of flow in a transonic compressor with a single circumferential casing groove: influence of groove location and depth on flow instability[J]. Journal of Turbomachinery, 2014, 136(3): 031017.

Sakuma Y, Watanabe T, Himeno T, et al. Numerical analysis of flow in a transonic compressor with a single circumferential casing groove: application to two different compressor rotors[C]. ASME Paper, GT2014-26691, 2014.

Mirzabozorg M A S, Bazazzadeh M, Hamzezade M. Numerical study on the effect of single shallow circumferential groove casing treatment on the flow field and the stability of a transonic compressor[J]. Journal of Applied Fluid Mechanics, 2017, 10(1): 257-265.

Takata H, Tsukuda Y. Stall margin improvement by casing treatment-its mechanism and effectiveness[J]. Journal of Engineering for Power, 1977, 99(1): 121-133.

Rolfes M, Lange M, Vogeler K, et al. Experimental and Numerical Investigation of a Circumferential Groove Casing Treatment in a Low-Speed Axial Research Compressor at Different Tip Clearances[J]. Journal of Turbomachinery, 2017, 139(12): 121009.

Hamzezade M, Agha Seyed Mirzabozorg M, Bazazzadeh M. Numerical study of the effect of the tip gap size and using a single circumferential groove on the performance of a multistage compressor[J]. Journal of Computational Applied Mechanics, 2019, 50(1): 54-62.

Beheshti B H, Teixeira J A, Ivey P C, et al. Parametric study of tip clearance–casing treatment on performance and stability of a transonic axial compressor[C]. ASME Paper, GT2004-53390, 2004.

Cevik M, Vo H D, Yu H. Casing treatment for desensitization of compressor performance and stability to tip clearance[J]. Journal of Turbomachinery, 2016, 138(12): 121008.

Reid L, Moore R D. Design and overall performance of four highly loaded, high speed inlet stages for an advanced high-pressure-ratio core compressor[R]. NASA Technical Paper, No.1337, 1978.

NUMECA International, IGG v8.7, User Manual,

Biollo R, Benini E. Shock/boundary-layer/tip-clearance interaction in a transonic rotor blade[J]. Journal of Propulsion and Power, 2009, 25(3): 668-677.

Gao L, Li X, Feng X, et al. The effect of tip clearance on the performance of contra-rotating compressor[C]. ASME Paper, GT2012-68801, 2012.

Vo H D, Tan C S, Greitzer E M. Criteria for spike initiated rotating stall[J]. Journal of Turbomachinery, 2008, 130(1):011023.

Cameron J D, Bennington M A, Ross M H, et al. The influence of tip clearance momentum flux on stall inception in a high-speed axial compressor[J]. Journal of Turbomachinery, 2013, 135(5): 051005.

Souleimani Y, Vo H D, Yu H. Performance desensitization for a high-speed axial compressor[C]. ASME Paper, GT2018-772031, 2018.

Rabe D C, Hah C. Application of casing circumferential grooves for improved stall margin in a transonic axial compressor[C]. ASME Paper, GT2002-30641, 2002.

Du J, Lin F, Chen J, et al. Flow structures in the tip region for a transonic compressor rotor[J]. Journal of Turbomachinery, 2013, 135(3): 031012.

Furukawa M, Inoue M, Saiki K, et al. The role of tip leakage vortex breakdown in compressor rotor aerodynamics[J]. Journal of Turbomachinery, 1999, 121(3): 469-480.

Schlechtriem S, Lötzerich M. Breakdown of tip leakage vortices in compressors at flow conditions close to stall[C]. ASME Paper, 97-GT-041, 1997.